Targeted disruption of *ATM* leads to growth retardation, chromosomal fragmentation during meiosis, immune defects, and thymic lymphoma

Yang Xu,[1] Terry Ashley,[3] Elizabeth E. Brainerd,[3] Roderick T. Bronson,[2] M. Stephen Meyn,[3,4] and David Baltimore[1,5]

[1]Department of Biology, Massachusetts Institute of Technology, Cambridge, Massachusetts 02139 USA; [2]Department of Pathology, Tufts University School of Medicine, Boston, Massachusetts 02111 USA; [3]Department of Genetics and [4]Department of Pediatrics, Yale University School of Medicine, New Haven, Connecticut 06510 USA

***ATM*, the gene mutated in the inherited human disease ataxia-telangiectasia, is a member of a family of kinases involved in DNA metabolism and cell-cycle checkpoint control. To help clarify the physiological roles of the ATM protein, we disrupted the *ATM* gene in mice through homologous recombination. Initial evaluation of the *ATM* knockout animals indicates that inactivation of the mouse *ATM* gene recreates much of the phenotype of ataxia-telangiectasia. The homozygous mutant ($ATM^{-/-}$) mice are viable, growth-retarded, and infertile. The infertility of $ATM^{-/-}$ mice results from meiotic failure. Meiosis is arrested at the zygotene/pachytene stage of prophase I as a result of abnormal chromosomal synapsis and subsequent chromosome fragmentation. Immune defects also are evident in $ATM^{-/-}$ mice, including reduced numbers of $B220^{+}CD43^{-}$ pre-B cells, thymocytes, and peripheral T cells, as well as functional impairment of T-cell-dependent immune responses. The cerebella of $ATM^{-/-}$ mice appear normal by histologic examination at 3 to 4 months and the mice have no gross behavioral abnormalities. The majority of mutant mice rapidly develop thymic lymphomas and die before 4 months of age. These findings indicate that the *ATM* gene product plays an essential role in a diverse group of cellular processes, including meiosis, the normal growth of somatic tissues, immune development, and tumor suppression.**

[*Key Words:* Meiosis; lymphoid development; tumorigenesis; DNA damage]

Received July 26, 1996; revised version accepted August 13, 1996.

Ataxia-telangiectasia (A-T) is a human autosomal recessive disease with a pleiotropic phenotype that includes growth retardation, cerebellar degeneration, oculocutaneous telangiectasias, and other progeric changes of the skin, endocrine dysfunction, gonadal abnormalities, immunodeficiency, high cancer risk, and hypersensitivity to ionizing radiation (Sedgwick and Boder 1991). There is no effective treatment for the underlying defect, and death from progressive neurologic degeneration or malignancy typically occurs in the second or third decade (Sedgwick and Boder 1991). Although A-T homozygotes are rare, the carrier frequency has been estimated to be ~1% in the U.S. population, and heterozygotes appear to be at increased risk for cancer, particularly breast carcinoma (for review, see Easton 1994; Meyn 1996). Although A-T homozygotes typically have no detectable neurologic abnormalities in the first year of life, they gradually lose cerebellar function, resulting in progressive ataxia, dysarthric speech, ocular apraxia, drooling, and choreoathetoid movements (for review, see Sedgwick and Boder 1991; Woods and Taylor 1992). Their functional neurologic abnormalities are accompanied by a continual loss of neurons from the central nervous system. The cerebellum is particularly affected owing to the cumulative effects of ongoing Purkinje cell death.

Most A-T patients develop secondary sexual characteristics; however, gonadal abnormalities associated with reduced numbers of germ cells are a characteristic feature of A-T (Sedgwick and Boder 1991). Female homozygotes have hypoplastic ovaries that rarely contain primordial follicles (Sedgwick and Boder 1991; McFarlin

[5]Corresponding author.

et al. 1972). Male homozygotes have been shown to have histological abnormalities of their testes with incomplete spermatogenesis or oligospermia (Aguilar et al. 1968; McFarlin et al. 1972; Agamanolis and Greenstein 1979), although the hypogonadism is less frequent and milder than in female homozygotes.

A-T patients exhibit both humoral and cellular immune defects, as indicated by thymic hypoplasia/aplasia, reduced numbers of circulating T cells, and a selective deficiency of immunoglobulin isotypes IgA, IgE, IgG_2 and IgG_4 (Peterson and Good 1968; Strober et al. 1968). The etiology of the immunoglobulin deficiency is unclear; it could be caused by intrinsic B-cell defects such as defective class-switch recombination or may be the result of helper T-cell dysfunction.

Cancer is frequent in A-T patients, and the tumor types are age-dependent (Spector et al. 1982). In A-T patients <15 years, the most common tumors are of lymphoid origin, but epithelial tumors tend to predominate beginning in late adolescence. Lymphoid tumors in young A-T patients are mainly of T-cell origin, and they frequently harbor the characteristic chromosome rearrangements seen in the circulating T lymphocytes of A-T patients (Kojis et al. 1991).

The chromosomal translocations and inversions seen in the lymphocytes and lymphoreticular malignancies of A-T patients typically involve four sites: 7p14, 7q35, 14q11.2, and 14q32. The translocation breakpoints interrupt the immunoglobulin and T cell receptor (*TCR*) genes contained in these chromosome bands (Kojis et al. 1991), suggesting that chromosomal translocations in the T lymphocytes of A-T patients may be attributable to illegitimate joining of these loci during V(D)J recombination. Spontaneous chromosome instability and high rates of spontaneous mitotic recombination have been documented in A-T cells from several different nonlymphoid organs (Bigbee et al. 1989; Kojis et al. 1991; Meyn 1993), indicating that widespread genetic instability is an intrinsic and generalized feature of the A-T phenotype.

Cells derived from A-T patients respond abnormally to certain types of DNA damage (for review, see Meyn 1995; Shiloh 1995) and lack DNA damage-sensitive cell-cycle checkpoint controls (Hartwell and Kastan 1994). Although the kinetics of induction and repair of double-stranded breaks are normal in A-T cells (for review, see Meyn 1995), they have higher than normal amounts of residual chromosome damage following irradiation (Pandita and Hittleman 1992) and difficulty in correctly rejoining double-stranded breaks in extrachromosomal plasmids (Cox et al. 1984; Ganesh et al. 1993), suggesting that A-T cells may have subtle defects in the handling of double-stranded breaks.

After the induction of double-stranded DNA breaks, normal cells typically halt at multiple checkpoints in the cell cycle, including the G_1/S border, S phase, and the G_2/M border (Hartwell and Kastan 1994). However, all three cell-cycle checkpoints are defective in A-T cells. The defective G_1/S checkpoint presumably is attributable to impaired p53 response after DNA strand-break damage (Kastan et al. 1992; Khanna and Lavin 1993; Xu and Baltimore, this issue). The basis for the S-phase and G_2/M checkpoint defects in A-T cells is unclear.

ATM, a gene mutated consistently in A-T patients, was identified through linkage mapping and positional cloning (Gatti et al. 1988; Savitsky et al. 1995). Sequence analysis of the *ATM* gene indicates that it codes for a 350-kD protein that is a member of a family of kinases involved in DNA metabolism and cell-cycle checkpoint control (Zakian 1995). Members of this family include the yeast proteins Rad3, Mec1, and Tel1; the Tor proteins; and their mammalian counterpart FRAP (Weinert and Lydall 1993; Brown et al. 1995; Greenwell et al. 1995; Hari et al. 1995; Morrow et al. 1995; Paulovich and Hartwell 1995). The greatest homologies between individual members of this family, including PI-3 kinase, occur at their carboxy-terminal kinase domain (Savitsky et al. 1995). The *ATM* gene shares similarities of protein sequence and mutant phenotype with these cell-cycle checkpoint genes, suggesting that ATM is involved in activating cell-cycle checkpoints and other cellular functions in response to spontaneous and induced DNA strand-break damage (Meyn 1995).

To understand the functions of ATM and the molecular basis for the A-T phenotype, we disrupted the *ATM* gene by homologous recombination (Xu and Baltimore, this issue). The mouse *ATM* homolog shares 84% amino acid identity and 91% similarity with human *ATM* (Pecker et al. 1996). Consistent with the defects seen in cells from A-T patients, embryonic fibroblasts (MEFs) derived from *ATM* homozygous mutant ($ATM^{-/-}$) mice are defective in the G_1/S cell-cycle checkpoint after DNA strand-break damage and exhibit defective cellular proliferation in culture, inefficient G_1 to S phase cell-cycle progression after serum stimulation, and premature senescence (Xu and Baltimore, this issue).

We now report the in vivo phenotype of the $ATM^{-/-}$ mice. They are viable but express postnatal growth retardation, have gonadal abnormalities, and are infertile. The basis of their infertility is the arrest of meiosis at prophase as a result of abnormal chromosomal synapsis and extensive chromosome fragmentation. The cerebella of $ATM^{-/-}$ mice appear normal by histologic examination, and the mice have no gross behavioral abnormalities. $ATM^{-/-}$ mice exhibit multiple immune defects similar to those of A-T patients. Most $ATM^{-/-}$ mice developed thymic lymphomas at 3 to 4 months of age and usually died of their tumors by 4 months. These findings demonstrate the involvement of ATM in multiple developmental processes, establish an essential role for ATM in meiosis, and document the utility of $ATM^{-/-}$ mice as an animal model for studying A-T.

Results

Growth defects in $ATM^{-/-}$ *mice*

To elucidate the normal functions of ATM, we disrupted the kinase domain of the *ATM* gene in mice through

homologous recombination. The sequence of the exons disrupted corresponded to the human *ATM* cDNA from nucleotides 8619 to 8831 (Savitsky et al. 1995; Xu and Baltimore, this issue). In addition, we cannot detect in $ATM^{-/-}$ cells any transcript through regions of the ATM kinase domain that were not disrupted directly, suggesting that there may be no expression of the gene (Xu and Baltimore, this issue). The $ATM^{-/-}$ mice are viable and slightly smaller than normal littermates before weaning at 3 weeks. At this age, the ratio of the body weights of $ATM^{-/-}$ mice versus the body weights of sex-matched $ATM^{+/+}$ littermates is 0.88 ± 0.05 (mean from 11 sets of $ATM^{+/+}$ and $ATM^{-/-}$ mice). However, by 5 weeks of age, the mutant animals exhibit a clear growth defect, being obviously smaller than normal littermates of the same sex. At this age, the ratio of the body weights of $ATM^{-/-}$ mice versus the body weights of sex-matched $ATM^{+/+}$ littermates is 0.76 ± 0.05 (mean from 15 sets of $ATM^{+/+}$ and $ATM^{-/-}$ mice). The differences in body weight between $ATM^{-/-}$ mice and controls persist through adulthood (data not shown). The defective growth in $ATM^{-/-}$ mice correlates with defective cellular proliferation observed in MEFs derived from $ATM^{-/-}$ mice (Xu and Baltimore, this issue). No growth defects were evident in $ATM^{+/-}$ mice (data not shown).

Spermatogenesis and oogenesis is disrupted in ATM$^{-/-}$ *mice*

Multiple attempts to breed $ATM^{-/-}$ mice with other $ATM^{-/-}$ mice or normal mice were unsuccessful. As oligospermia and testicular abnormalities are a frequent finding in male A-T patients, we compared the histologic development of the seminiferous tubules of testes from $ATM^{-/-}$ mice with those from normal mice. As expected, the seminiferous tubules of 6-week-old normal mice contained cells in all stages of spermatogenesis, including spermatogonia (stem cells), spermatocytes, and round and fully elongated spermatids (Fig. 1A,C). The spermatogonia form a peripheral cell layer with primary spermatocytes lying just interior to the spermatogonia. Both round spermatids with light-staining nuclei and fully elongated spermatids with tails extending into the lumen are easily identified in the seminiferous tubules of $ATM^{+/+}$ mice. In contrast, although the spermatogonia appear relatively normal in the seminiferous tubules of 6-week-old $ATM^{-/-}$ males, spermatocytes are found in various stages of degeneration and round or elongated spermatids are completely absent (Fig. 1B,D). Morphologically, spermatocytes in $ATM^{-/-}$ mice appear to halt development between the zygotene and pachytene stages of meiotic prophase (Fig. 1D), suggesting that meiotic arrest in $ATM^{-/-}$ mice occurs in early prophase.

A similar picture is seen with histologic examination of the ovaries from $ATM^{-/-}$ mice. Although ovaries from 5- to 6-week-old normal mice have primary oocytes and follicles of different maturation stages (Fig. 1E,G), ovaries from $ATM^{-/-}$ females are highly degenerate and

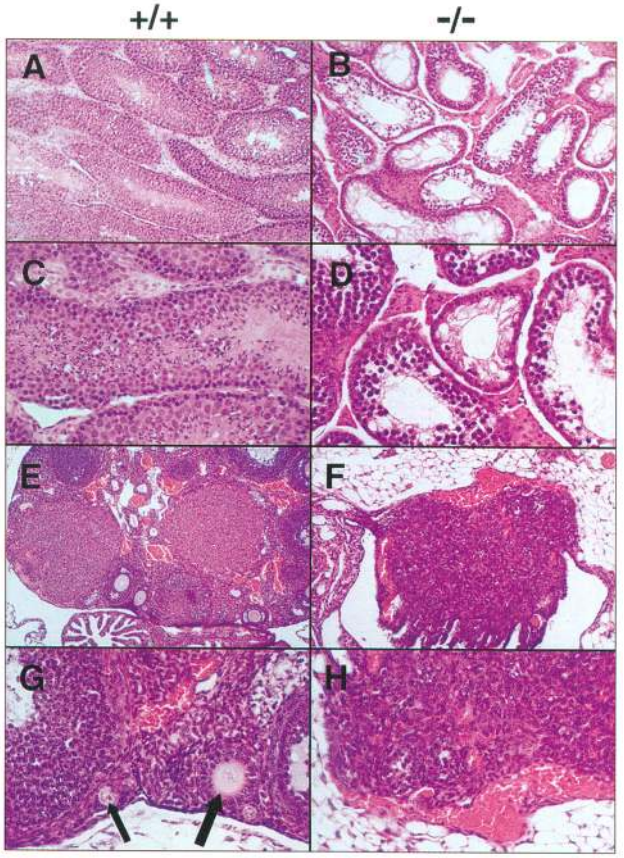

Figure 1. Defective spermatogenesis and oogenesis in $ATM^{-/-}$ mice. (*A–D*) Histological sections of seminiferous tubules of 6- to 7-week-old $ATM^{+/+}$ (*A,C*) and $ATM^{-/-}$ (*B,D*) littermates were stained with hematoxylin–eosin. (*E–F*) Hematoxylin–eosin-stained sections of ovaries derived from 5-week-old $ATM^{+/+}$ (*E,G*) and $ATM^{-/-}$ (*F,H*) mice. (*E,F*) show the gross ovarian morphology. (*G,H*) show follicles containing immature oocytes at a higher magnification. The primary oocytes indicated with a thin arrow and immature follicles indicated with a thick arrow are present in $ATM^{+/+}$ ovary but completely absent in $ATM^{-/-}$ ovary. (*A,B,E,F*) Magnification, 50×; (*C,D,G,H*) magnification, 100×.

contain no primary oocytes or follicles (Fig. 1F,H). As oocytes in normal mice arrest in dictolate, a post-pachytene stage of meiosis, this observation suggests that meiosis is disrupted before normal meiotic arrest in $ATM^{-/-}$ females.

Meiosis is blocked at the zygotene/pachytene stage during spermatogenesis in ATM$^{-/-}$ *mice*

To follow meiotic events, we used a polyclonal antibody against the Cor1 protein, a component of the axial/lateral element of the synaptonemal complex (Dobson et al. 1994). In normal spermatocytes, Cor1 is detected first as the axial elements form between sister chromatids during leptonema. It remains a part of the synaptonemal complex through homologous synapsis during zygonema (Fig. 2A,C,E), full synapsis during pachynema (6 days in

spermatocytes) (Fig. 2G), and desynapsis and separation of homologs, disappearing only as the lateral elements disassemble in diplonema (Dobson et al. 1994).

In $ATM^{-/-}$ mice, the earliest substages of meiotic prophase (leptonema, early zygonema) appear normal when monitored by Cor1. However, there are clear irregularities in mid-zygotene nuclei. In normal mice, synapsis begins typically at the distal ends of the acrocentric chromosomes and proceeds zipper-fashion toward the centromeric ends; interstitial synaptic initiation is rare. In contrast, in zygotene nuclei from $ATM^{-/-}$ male mice, there are frequently interstitial points of contact between apparent homologs with asynapsis on either side of the contact (Fig. 2B, arrows). These aberrant interstitial synapses are not the rule, however, in that many bivalents in $ATM^{-/-}$ zygotene nuclei appear normal, as monitored by Cor1, with synapsis proceeding from the distal to the proximal end. Nonetheless, there are far more univalents and partially synapsed bivalents in $ATM^{-/-}$ zygotene spermatocytes than in zygotene spermatocytes from normal mice (cf. Fig. 2B,D, $ATM^{-/-}$ nuclei, with Fig. 2A,C, normal nuclei). In addition, in normal spermatocytes, the axial element forms only slightly in advance of the complete synaptonemal complex; whereas in the $ATM^{-/-}$ spermatocytes there are extensive unpaired axial elements. Taken together, these observations suggest that there is a general delay in synapsis in $ATM^{-/-}$ spermatocytes.

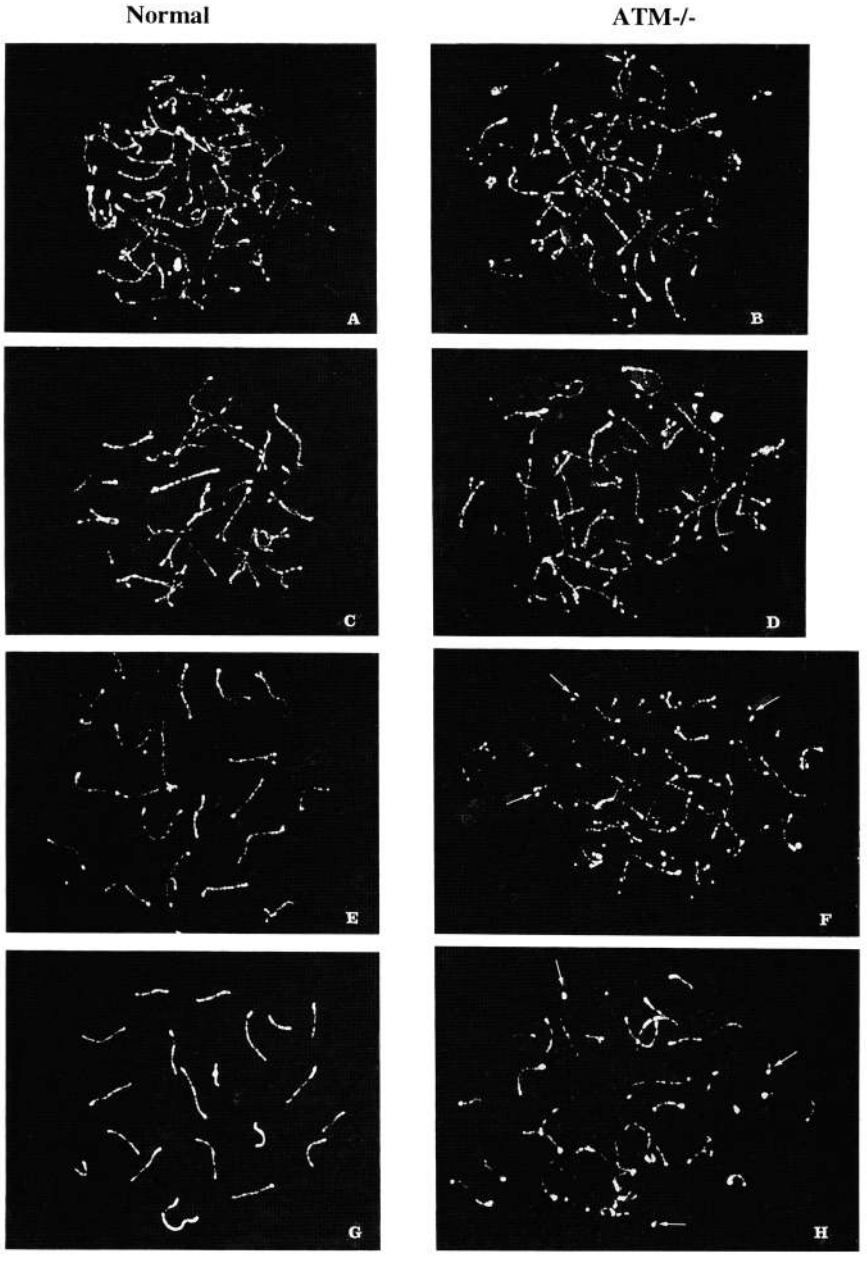

Figure 2. Comparison of progressively later zygotene and pachytene stages of normal spermatocytes (*left*) and $ATM^{-/-}$ spermatocyte (*right*). (*A,C*) Normal zygotene nuclei stained with the Cor1 antibody showing progressive synapsis of bivalents from distal to proximal ends. (*B,D*) Similar stages of nuclei in $ATM^{-/-}$ spermatocytes showing interstitial initiation of synapsis indicated by arrows. (*E,G*) A very late normal zygotene nucleus (*E*) with synapsis nearly complete and a normal mid-pachytene nucleus (*G*) with all autosomes fully synapsed. (*F,H*) Aberrant "pachytene" nuclei from $ATM^{-/-}$ spermatocytes. Chromosome fragments are indicated with arrows.

Despite these apparent abnormalities, most $ATM^{-/-}$ nuclei progress into pachynema, although this stage is highly aberrant. Most bivalents are synapsed, but they are fragmented. In addition to larger axial segments that might represent theoretically complete bivalents, we see 15–20 small axial pieces per "early pachytene" nucleus (Fig. 2F,H). This number represents approximately one fragment per bivalent. However, the more degenerate a nucleus appears, the more fragments we observe, indicating progressive chromosome damage resulting in fragmentation and erosion of the entire genome. These nuclei appear morphologically apoptotic and late pachytene or postpachytene stages are never observed, suggesting complete nuclear degeneration and cellular death during pachynema.

Lack of cerebellar degeneration in $ATM^{-/-}$ *mice*

As progressive cerebellar degeneration leading to ataxia is a characteristic defect seen in A-T patients, we examined the histologic sections of brains obtained from 1- to 4-month-old $ATM^{-/-}$ mice. No obvious histologic abnormalities were detected, including structural defects, generalized cerebellar degeneration, or specific loss of Purkinje cells (data not shown). $ATM^{-/-}$ mice did not display overt ataxia or other readily discernible abnormal behaviors.

Defective immune development in $ATM^{-/-}$ *mice*

Because most A-T patients suffer from immune defects, we examined lymphoid development in 5- to 7-week-old $ATM^{+/+}$, $ATM^{+/-}$, and $ATM^{-/-}$ littermates. Histologically, the structures of the thymus and spleen remain intact in $ATM^{-/-}$ mice, although thymuses of $ATM^{-/-}$ mice are consistently smaller than those of normal littermates (data not shown). The number of thymocytes in $ATM^{-/-}$ mice averages <40% that of $ATM^{+/+}$ littermates of the same sex (Fig. 3B). As determined by flow cytometric analysis for CD4 and CD8 markers, the absolute numbers of single positive (SP) and double positive (DP) thymocytes are reduced in the $ATM^{-/-}$ animals and there is a particular reduction in the relative proportion of $CD4^+$ SP thymocytes (Fig. 3). The reduction of mature SP thymocytes correlates with a large reduction of T cells in the peripheral lymphoid organs of $ATM^{-/-}$ mice (Fig. 3A; data not shown). The reduced number of thymocytes in $ATM^{-/-}$ mice does not appear to be attributable to fewer T-lineage precursors, as the absolute number of $CD4^-$ $CD8^-$ (DN) thymocytes in $ATM^{-/-}$ mice is similar to that in $ATM^{+/+}$ mice (Fig. 3B,C).

We also observed an intermediate reduction of total thymocyte number in $ATM^{+/-}$ mice (Fig. 3A,B). However, because the percentage of SP thymocytes is increased compared with that of normal mice, the absolute number of SP thymocytes is similar in the thymi of $ATM^{+/+}$ and $ATM^{+/-}$ littermates (Fig. 3B,C). Therefore, the reduction of total thymocytes reflects an ~30% reduction in the absolute number of DP thymocytes (Fig. 3).

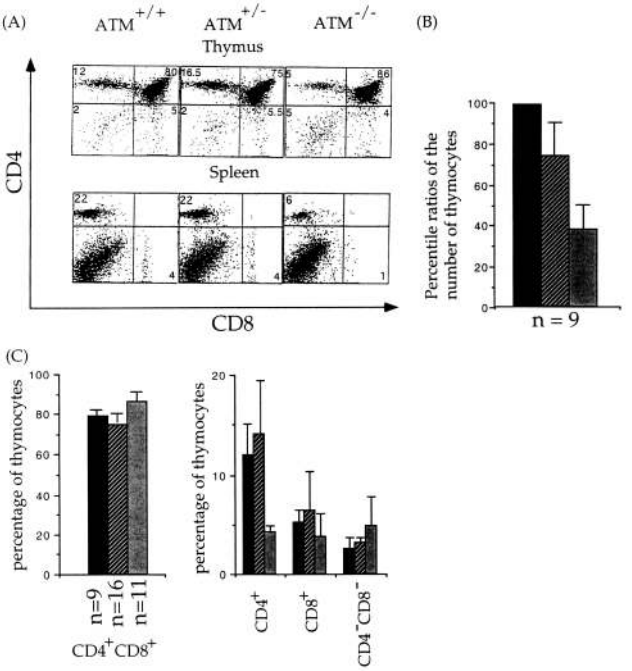

Figure 3. T-cell development in $ATM^{-/-}$ mice. (*A*) Flow cytometric analysis of the cells derived from thymus and spleen of 6-week-old $ATM^{+/+}$, $ATM^{+/-}$, and $ATM^{-/-}$ mice. Cells residing in the lymphocyte gate were analyzed and the percentage of total cells in a particular gate is indicated. Consistent data were obtained from nine independent experiments. (*B*) The percentile ratios of the number of thymocytes in $ATM^{+/-}$ or $ATM^{-/-}$ mice versus the number of thymocytes in $ATM^{+/+}$ littermates of the same sex. (Solid bar) $ATM^{+/+}/ATM^{+/+}$; (hatched bar) $ATM^{+/-}/ATM^{+/+}$; (shaded bar) $ATM^{-/-}/ATM^{+/+}$. n represents how many sets of mice were analyzed and the mean value is presented with error bars. (*C*) The percentage of subpopulations of thymocytes in the thymus of $ATM^{+/+}$ (solid bar), $ATM^{+/-}$ (hatched bar), and $ATM^{-/-}$ (shaded bar) mice. n represents the number of mice analyzed and the mean value is presented with error bars.

Similar to the developmental defects of thymocytes in $ATM^{-/-}$ mice, the number of $B220^+IgM^-$ pre-B cells were also decreased when the bone marrow of $ATM^{-/-}$ mice was compared to that of $ATM^{+/+}$ littermates (Fig. 4B). The ratio of $B220^+IgM^-$ pre-B cells in the bone marrow of $ATM^{-/-}$ mice to those of $ATM^{+/+}$ mice is 0.63 ± 0.17 (mean of eight independent pair-wise comparisons of $ATM^{-/-}$ and $ATM^{+/+}$ mice). The reduction in numbers of pre-B cells was not attributable to fewer progenitors committed to the B lineage, because similar numbers of $B220^+CD43^+$ pre-B cells were present in the bone marrow of $ATM^{+/+}$ and $ATM^{-/-}$ mice (Fig. 4B). The ratio of $B220^+CD43^+$ pro-B cells in the bone marrow of $ATM^{-/-}$ mice to those of $ATM^{+/+}$ mice is 0.97 ± 0.13 (mean from six independent pair-wise comparisons). The higher percentage of granulocytic and ery-

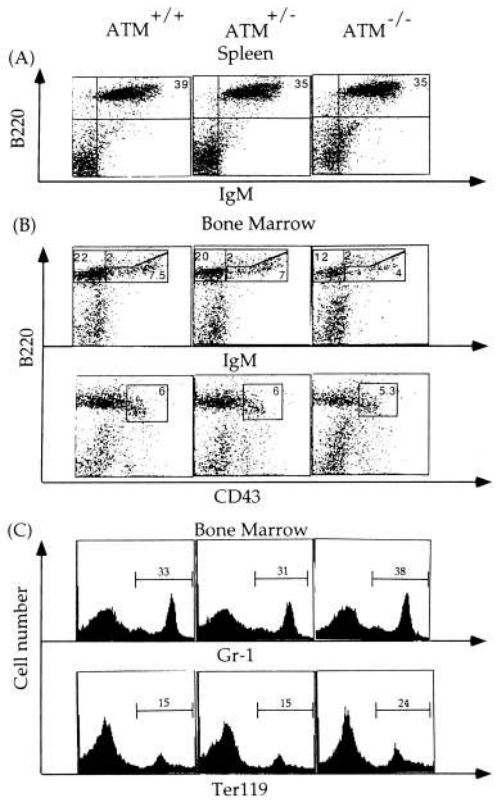

Figure 4. Flow cytometric analysis of B cell and other hematopoietic lineage cells in the spleen (*A*) and bone marrow (*B,C*) of $ATM^{+/+}$, $ATM^{+/-}$, and $ATM^{-/-}$ mice. In *A* and *B*, cells residing in lymphoid gate were analyzed and the percentage of total cells in a particular gate is indicated. Consistent data on the B cells in the spleen were obtained in nine independent experiments.

throid lineage cells in the bone marrow of $ATM^{-/-}$ mice is likely attributable to decreased numbers of B-lineage cells in the bone marrow of these mice (Fig. 4C). Unlike the defects in the T-lineage cells, no reduction of pre-B cells were detected in the bone marrow of $ATM^{+/-}$ mice and similar number of B-cells were present in the spleens of $ATM^{+/+}$, $ATM^{+/-}$, and $ATM^{-/-}$ mice (Fig. 4A,B).

Immunoglobulin isotype levels and immune response in ATM$^{-/-}$ *mice*

Because mature B and T cells are present in $ATM^{-/-}$ mice, we examined the immune response of $ATM^{-/-}$ mice to T-dependent and T-independent antigens. The T-dependent immune response to NP_{15}-CG was impaired in $ATM^{-/-}$ mice, whereas a normal T-dependent immune response was detected in $ATM^{+/-}$ mice (Fig. 5A). However, the T-independent immune response to NP-Ficoll in $ATM^{-/-}$ mice was normal (Fig. 5B). B cells derived from $ATM^{-/-}$ mice proliferated normally in vitro in response to stimuli including anti-IgM antibody, lipopolysaccharide (LPS), and CD40 ligand (data not shown). These observations suggest that B cells in $ATM^{-/-}$ mice are functionally normal. Therefore, an impaired T-dependent immune response in $ATM^{-/-}$ mice likely is attributable to defective functioning of helper T cells or interrupted T cell–B cell interactions.

Because A-T patients exhibit a selective deficiency of immunoglobulin isotypes, we analyzed the serum levels of IgM, IgG subclasses, and IgA. The serum levels of immunoglobulin isotypes are grossly similar between $ATM^{+/+}$ and $ATM^{-/-}$ mice (Table 1). However, there is a 1.5- to 2-fold reduction of the serum levels of IgG_{2a}, IgG_{2b}, IgG_3 in the mutants (Table 1).

Thymic lymphomas in ATM$^{-/-}$ *mice*

By 3 months of age, most $ATM^{-/-}$ mice have developed thymic lymphomas. However, we have not observed an increased frequency of other malignancies in $ATM^{-/-}$ mice, possibly because they all succumb to thymic disease. The onset of thymic lymphoma appears to be quite early, as tumors with highly proliferating lymphoblasts have been detected in 1- to 2-month-old $ATM^{-/-}$ mice

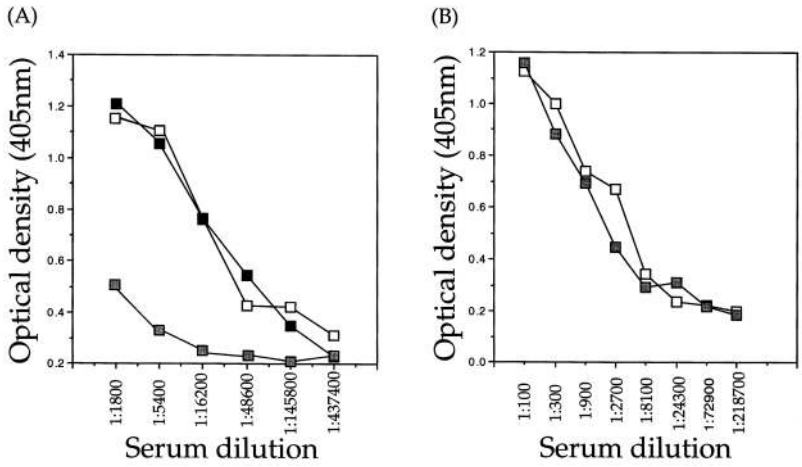

Figure 5. T-dependent and T-independent immune responses in $ATM^{-/-}$ mice. (*A*) Impaired immune response to T-dependent antigens in $ATM^{-/-}$ mice. Serial dilutions of serum (1800× initial dilution and threefold dilution at each subsequent points) were analyzed for NP-specific IgG. Results are presented as OD_{405} of anti-IgG-specific ELISA using BSA-NP as capturing antigen. Consistent results were obtained from three mice of each genotype. (*B*) T-independent immune response in $ATM^{-/-}$ mice. Serial dilutions of serum (100× initial dilution and threefold dilution at each subsequent points) were analyzed for NP-specific total immunoglobulin. Consistent results were obtained from five sets of $ATM^{+/+}$ and $ATM^{-/-}$ mice. (*A,B*) (Open box) $ATM^{+/+}$; (solid box) $ATM^{+/-}$; (shaded box) $ATM^{-/-}$.

Table 1. *Serum concentrations of immunoglobulin isotypes from 6-week-old* $ATM^{+/+}$ *and* $ATM^{-/-}$ *mice*

	Ig isotypes (μg/ml)					
Genotype	IgM	IgG_1	IgG_{2a}	IgG_{2b}	IgG_3	IgA
$ATM^{+/+}$	1205 ± 428	1308 ± 697	640 ± 322	668 ± 278	206 ± 23	256 ± 66
$ATM^{-/-}$	1532 ± 640	1170 ± 427	325 ± 169	400 ± 194	116 ± 58	308 ± 91
P value	0.323	0.688	0.060	0.082	0.006	0.284

Mean values with standard deviations from six pairs of $ATM^{+/+}$ and $ATM^{-/-}$ littermates are presented along with *P* values for *t*-test comparisons of the serum isotype concentrations.

(data not shown). The rapidly growing lymphomas disrupt completely the cortical–medullary structure of the normal thymus and eventually fill the chest cavity, leading to collapse of the lung and death of the animal, usually by 4 months of age (Fig. 6). Although a large number of tumor cells circulate in the blood, they fail to infiltrate any nonlymphoid tissues, including lung and heart (data not shown). Flow cytometric analysis of the tumor cells indicates that these cells are invariably of $CD4^+CD8^+$ DP origin and composed of large-sized lymphoblasts (Fig. 7A). Furthermore, the tumor cells are heat stable antigen $(HSA)^{high}$, further confirming that these tumors originate from immature thymocytes (Fig. 7A).

Normally, DP thymocytes already have rearranged their *TCRβ* locus (von Boehmer 1994). Therefore, to test the clonality of the tumor cells we used a PCR assay to study the TCRβ chain structure in the tumor cells (Winandy et al. 1995). The PCR primers, specific for the Dβ2 and Jβ2.7 segments, amplified seven Dβ2–Jβ2 rearrangements from normal thymocytes, reflecting the polyclonal nature of thymocytes in normal mice (Fig. 7B and C, lane 2). In contrast, in most cases, tumor cells from the $ATM^{-/-}$ mice displayed only one predominant Dβ2–Jβ2 rearrangement, indicating a clonal origin (Fig. 7C). Genomic DNAs that contained two predominant Dβ2–Jβ2 rearrangements may be from tumors that are oligoclonal or from tumor cells containing DJ rearrangements on both alleles.

Frequently, lymphomas and leukemias in A-T patients frequently harbor chromosome rearrangements involving the *TCR* genes (Kojis et al. 1991), raising the possibility of similar rearrangements in the thymic lymphomas of $ATM^{-/-}$ mice. Because it is difficult to identify chromosomal translocations in the mouse by standard karyotypic methods, we used Southern blotting to assay for translocations involving the *TCRβ* locus in the tumor cells. Samples of genomic DNA isolated from thymic lymphoma cells, normal thymocytes, and embryonic stem cells were digested with *Eco*RI and then probed with a 900-bp genomic fragment containing the *TCRβ* enhancer (Fig. 7B). The germ-line *Eco*RI fragment is 9.5 kb, and translocation into this *Eco*RI fragment could generate restriction fragments of different sizes (Fig. 7B). Among six tumors assayed, one exhibited a smaller *Eco*RI restriction fragment in addition to the

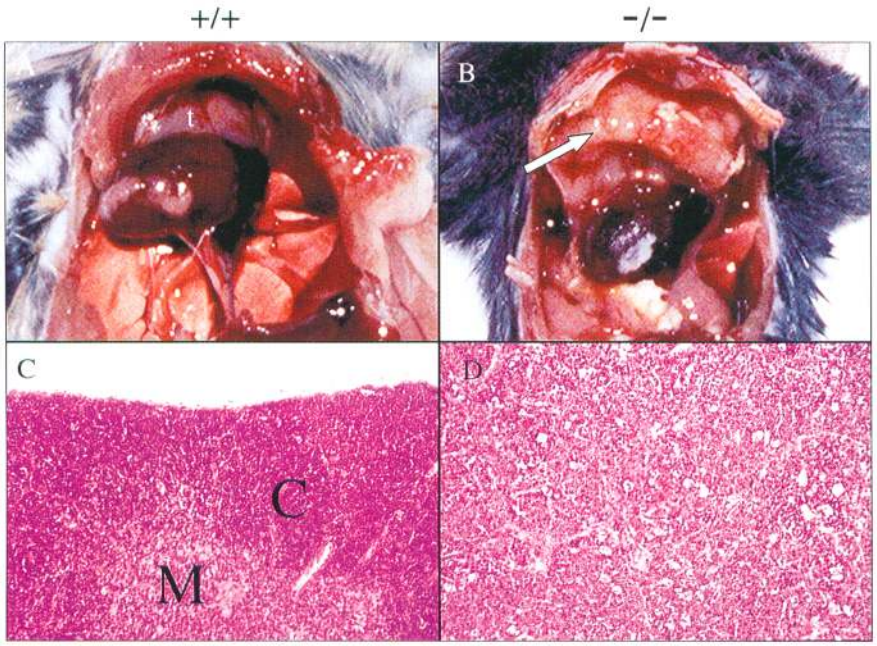

Figure 6. Histological analysis of thymic lymphomas in $ATM^{-/-}$ mice. Physical appearance of normal thymus (*A*) and thymic lymphoma (*B*) of 3-month-old animals. (t) Normal thymus; (arrow) thymic lymphoma. (*C,D*) Hematoxylin–eosin-stained sections of the normal thymus (*C*) and thymic lymphoma (*D*). The structure of cortex (C) and medulla (M) is absent in the lymphomic thymus.

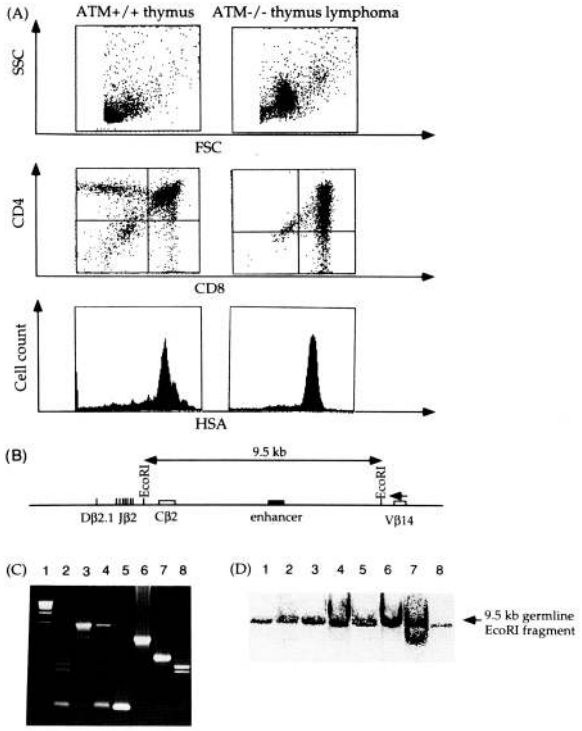

Figure 7. Analysis of thymic lymphoma in $ATM^{-/-}$ mice. (*A*) Representative FACScan profile of thymic lymphoma in $ATM^{-/-}$ mice. Thymocytes derived from a lymphoma in a 3-month-old $ATM^{-/-}$ mouse and those from a healthy littermate were analyzed for the surface expression of CD4, CD8, and heat stable antigen (HSA). Plots with the FSC (*x* axis) versus SSC (*y* axis) indicate the uniform and large-sized blasting lymphoma cells in these thymuses. (*B*) Germ-line configuration of *Dβ2–Jβ2–Cβ2*–TCR*β* enhancer locus (Malissen et al. 1986). The *TCRβ* enhancer is indicated with a filled box and the 9.5-kb *Eco*RI fragment is shown. (*C*) PCR analysis of Dβ2–Jβ2 rearrangements in cells derived from normal thymus and thymic lymphoma. Expected size of PCR products for the rearrangement of Dβ2 to seven Jβ2 is between 224 bp and 1279 bps (Winandy et al. 1995). (Lane *1*) 1-kb DNA size marker (GIBCO); (lane *2*) normal thymus; (lanes *3–8*) thymic lymphoma. The amplified PCR products were verified by Southern blot using an internal oligonucleotide as probe. (*D*) Southern blot analysis to assay for chromosomal translocation to the *TCRβ* enhancer region. Genomic DNA isolated from normal cells and tumors were digested with *Eco*RI and hybridized with a probed derived from the *TCRβ* enhancer. (Lane *1*) Embryonic stem cells; (lane *2*) normal thymocytes; (lanes *3–8*) thymic lymphoma.

germ-line *Eco*RI fragment, suggesting an aberrant genomic rearrangement involving the *Eco*RI fragment of the *TCRβ* enhancer on one chromosome (Fig. 7D, lane 7). The other tumor cells also may contain chromosomal translocations that cannot be detected by this particular combination of enzyme digestion and probe.

Discussion

We have created *ATM* mutant mice by targeted disruption of two exons encoding the kinase-conserved sequence but found no evidence of expression of the truncated mRNA beyond the disrupted exons, suggesting that no stable RNA is made from the partially deleted gene (Xu and Baltimore, this issue). Therefore, the phenotypes of the mutant mice may reflect the full range of activities of ATM.

Mice homozygous for this mutation express several in vivo aspects of the A-T phenotype, including growth retardation, gonadal abnormalities, immune defects, and a high incidence of T cell lymphomas. Furthermore, primary cells derived from these $ATM^{-/-}$ mice display cellular defects characteristic of A-T, such as hypersensitivity to γ-irradiation, defective cell-cycle checkpoint control, and premature senescence (Xu and Baltimore, this issue). Neither ataxia nor telangiectasia has been observed in young $ATM^{-/-}$ animals. Therefore, the $ATM^{-/-}$ mouse represents at least a partial animal model for A-T and the key aspects of the human condition that have yet to be evident may appear if the early-onset lymphomas can be suppressed. Consistent with findings in A-T patients that mutations throughout the *ATM* gene result in similar phenotypic defects, an independently generated $ATM^{-/-}$ mouse line—reported while this communication was in preparation—in which an insertional mutation was introduced 5′ of the kinase domain, exhibits similar defects to those we observe in our $ATM^{-/-}$ mice (Barlow et al. 1996).

To explain the pleiotropic defects in $ATM^{-/-}$ mice, we first consider the possible roles of ATM in repair of DNA double-stranded breaks. ATM is a member of a family of large kinases that mediate cell-cycle checkpoints. ATM appears to be involved specifically in sensing double-stranded breaks in DNA and signaling efficient cell-cycle arrest after this particular type of DNA damage (Meyn 1995). As suggested by the only recognizable motif, the kinase domain, and its large size, ATM could exert this function by activating DNA repair pathways through protein phosphorylation and protein–protein interactions. However, as suggested by its similarity to the DNA–PK catalytic subunit, ATM also could play a direct role in processing or repair of DNA damage, perhaps by interacting with DNA double-stranded breaks after complexing with proteins related functionally to the Ku subunits of DNA–PK (Blunt et al. 1995; Kirchgessner et al. 1995).

Several aspects of the phenotype of *ATM* mutant mice could be explained by the involvement of ATM in the cellular response to double-stranded DNA breaks. Lymphocytes mature through a process of DNA rearrangement of V(D)J gene segments involving double-stranded breaks (Blackwell and Alt 1989). V(D)J recombination appears to be restricted to the G_0/G_1 phase of the cell cycle, perhaps so as to preserve the chromosomal integrity of lymphocytes by insuring that rearrangement-induced double-stranded breaks are not present during S phase (Lin and Desiderio 1995). Double-stranded breaks during V(D)J recombination might activate ATM-dependent cellular functions that could halt the cell cycle until V(D)J recombination is completed (Meyn 1995). Therefore, in the absence of ATM activity, lymphocytes could enter S phase before V(D)J recombination is com-

pleted, possibly leading to a decreased frequency of productive V(D)J recombination. Because expression of productively rearranged Igμ chain and TCRβ chain is required for expansion of pre-B cells and DP thymocytes (Kitamura et al. 1992; Mombaerts et al. 1992; Shinkai et al. 1993; Feling et al. 1995; Xu et al. 1996b), the hypothesis that defective cell-cycle arrest during V(D)J recombination leads to a decreased frequency of productive V(D)J recombination could explain our observations that both pre-B cells and DP thymocytes are reduced in $ATM^{-/-}$ mice. Furthermore, this hypothesis could also account for the markedly reduced mature SP thymocytes in $ATM^{-/-}$ mice because only DP thymocytes with mature TCR on the surface can be selected positively to differentiate into mature SP thymocytes (Boehmer 1994). Alternatively, the primary cause for the reduced pre-B cells and thymocytes could be defective cellular proliferation, as has been observed in $ATM^{-/-}$ MEFs (Xu and Baltimore, this issue).

Lack of cell-cycle checkpoint control during V(D)J recombination in $ATM^{-/-}$ thymocytes may also contribute to an increased frequency of chromosomal translocations and inversions, which in turn could lead to deregulated expression of proto-oncogenes. In support of this idea, an aberrant genomic rearrangement involving the *TCRβ* locus was detected in one of the six thymic lymphomas examined. In addition, DP thymocytes are more resistant than normal thymocytes to early-onset apoptosis induced by DNA double-stranded breaks (Xu and Baltimore, this issue). This resistance might allow $ATM^{-/-}$ thymocytes with damaged DNA to survive and undergo selection for mutant cells that are neoplastic. Why thymocytes are more susceptible to tumorgenesis than B cells is not clear, but mouse B cells may have alternative means of handling DNA damage, because many carcinogens and oncogenes can selectively induce T cell tumors in mice (Newcomb et al. 1989; Janowski et al. 1990).

The meiotic defect in $ATM^{-/-}$ mice is also explicable in this framework. Histologic examination of the gonads from our $ATM^{-/-}$ mice demonstrated an absence of mature gametes in both ovaries and testes, findings similar to those reported for the *ATM* knockout mouse developed by Barlow et al. (1996). Confirmation that functional ATM protein is essential for meiosis is provided by the observations of ATM at sites along synapsed chromosomal axes (Keegan et al., this issue) and our finding that meiotic chromosome behavior is abnormal in the spermatocytes of $ATM^{-/-}$ mice. Mutations in the *Saccharomyces cerevisiae MEC1* and *Drosophila melanogaster mei41* checkpoint genes also express defects in meiotic recombination (Baker and Carpenter 1972; Kato and Ogawa 1994), suggesting that ATM is one of several members of this PI-3 kinase-related family of mitotic cell-cycle checkpoint proteins that play critical roles in the meiotic cell cycle.

Despite the finding that the most striking meiotic defect in $ATM^{-/-}$ mice is chromosome fragmentation, by the time that we can observe these fragments, the nuclei are already highly aberrant. Although $ATM^{-/-}$ spermatocytes appear incapable of preventing or repairing the damage that gave rise to these fragments, the fragments themselves are most likely the consequence of an earlier event. Antibody localization studies recently have shown that ATM protein associates with mouse spermatocyte chromosomes during meiosis (Keegan et al., this issue). Foci of ATM protein are detected first in association with meiotic chromosomes beginning in early zygonema as homologs synapse (Keegan et al., this issue), a time when the initial ATM-related disruption of meiotic events might occur in $ATM^{-/-}$ mice. Indeed, it is during this initial stage of synapsis that we first detect abnormalities in the $ATM^{-/-}$ spermatocytes.

It is possible that, like its homolog DNA–PK_{cs} (Anderson 1993), ATM binds to double-stranded DNA breaks or nicks. Because double-stranded breaks are thought to occur in meiotic prophase as an obligatory step of meiotic recombination (Sun et al. 1989; Cao et al. 1990), the ATM foci seen associated with synapsed meiotic chromosomes might be sites of double-stranded breaks. If so, then ATM might be a component, along with Rad51, of the molecular machinery that carries out one or more steps of synapsis and recombination. In this model, lack of functional ATM would directly disrupt chromosome pairing and compromise the integrity of synapsed chromosome, allowing conversion of nascent double-stranded breaks into chromosome breaks.

In addition, or alternatively, ATM may play a key role in a signal transduction network that activates checkpoints and other cellular responses to DNA strand breaks during meiosis (Meyn 1995; Shiloh 1995). Because ATM is required for activation of the S-phase checkpoint by double-stranded breaks in somatic cells (Kastan et al. 1992; Khanna and Lavin 1993; Canman et al. 1994), it is likely that ATM regulates one or more aspects of mitotic DNA replication. Plug et al. (1996) recently demonstrated the occurrence of DNA synthesis at meiotic pairing forks as homologous chromosomes synapse. The localization of ATM to similar foci at pairing forks at the time that this DNA synthesis is occurring raises the intriguing possibility that ATM controls a meiotic checkpoint that regulates zygotene DNA synthesis. The loss of this or other ATM-dependent meiotic checkpoints may prevent the proper coordination of molecular events necessary to maintain chromosome pairing. Loss of these checkpoints may also allow double-stranded DNA breaks or related structures normally present in synapsed chromosomes to be converted to chromosome breaks, resulting in fragmentation of the genome and the death of germ cells during pachynema. This is also the stage in meiosis at which most chromosome aberrations, and other genomic abnormalities that result in pairing problems, arrest in multicellular eukaryotes (de Boer and de Jong 1989; Jenkins 1989; Speed 1989).

There are other effects of *ATM* mutation seen thus far more prominently in humans than in mice. These are ataxia and telangiectasia. We have yet to detect any neurological defects, including cerebellar degeneration leading to ataxia, in $ATM^{-/-}$ mice as old as 4 months of age. This could be because the onset and rate of cerebellar

development is different between mice and humans (Jacobson 1991). In humans, the cerebellum is fully developed at birth, whereas the mouse cerebellum only becomes fully developed 1 month after birth. Therefore, longer times than 4 months may be needed for $ATM^{-/-}$ mice to develop detectable neurological defects. Alternatively, more sophisticated behavioral tests may be needed to uncover subtle behavioral abnormalities, if present, in the $ATM^{-/-}$ mice. In this regard, it should be noted that the $ATM^{-/-}$ mice created by Barlow et al. (1996) also lack gross ataxia but performed relatively poorly in specific tests of coordination and motor function.

Because several epidemiological studies have concluded that heterozygote carriers of *ATM* mutations are at increased risk to develop cancer (for review, see Easton 1994; Meyn 1996), we studied the behavior of cells derived from $ATM^{+/-}$ mice as well as various developmental processes in $ATM^{+/-}$ mice. Compared with cells from $ATM^{+/+}$ and $ATM^{-/-}$ littermates, cells from $ATM^{+/-}$ mice have an intermediate impairment in their γ-radiation-induced G_1/S cell-cycle arrest, but proliferate normally in culture. In addition, immature $ATM^{+/-}$ thymocytes are more resistant to γ-irradiation than immature normal thymocytes, suggesting that $ATM^{+/-}$ mice may be more susceptible to tumorgenesis induced by DNA damage (Xu and Baltimore, this issue). The $ATM^{+/-}$ mice appear normal in several aspects of animal development. Their growth is indistinguishable from normal littermates, and they are fertile and immune competent. However, there is an intermediate reduction in the number of immature thymocytes in these animals. We have not observed an increased incidence of malignancies in $ATM^{+/-}$ mice as old as 6 months of age, but we are testing the possibility that γ-irradiation will unmask any increased tendency of $ATM^{+/-}$ mice to develop tumors.

Materials and methods

Histologic analysis

Harvested tissues were fixed in buffered formalin (from J.T. Baker, Philipsburg, NJ), dehydrated, and embedded in paraffin. Sagittal sections were cut and stained with hematoxylin–eosin, and examined by light microscopy.

Immunochemical studies of meiotic nuclei

More than 150 nuclei were imaged from three 3-week-old $ATM^{-/-}$ males. Surface spreads from spermatocytes were prepared using the method of Speed (1982) as modified by Antoine Peters (pers. comm.). The Cor1 antibody is a polyclonal antibody raised in mouse directed against the Cor1 protein from Syrian hamster (Dobson et al. 1994). Cor1 is a component of the axial/lateral elements of the synaptonemal complex and the antibody has been shown to be specific for these components (Dobson et al. 1994). The method of detection was as described in Ashley et al. (1995).

Flow cytometric analysis of hematopoietic cells

Single-cell suspensions were prepared from thymus, spleen, and bone marrow as described previously (Xu et al. 1996a). Cells were diluted in 0.2% acetic acid to lyse the red blood cells and counted with a hemacytometer. For two-color flow cytometry analysis, 5×10^5 cells were stained in each reaction. Thymic or splenic cells were stained simultaneously with PE-conjugated anti-CD4 antibody and FITC-conjugated anti-CD8 antibody; splenic cells were also stained with PE-conjugated anti-B220 antibody and biotinylated anti-IgM antibody; bone marrow cells were stained with PE-conjugated anti-B220 and biotinylated anti-IgM antibody or biotinylated anti-CD43 antibody for detection of B-lineage cells. The bone marrow cells were also stained with biotinylated anti-Gr-1 antibody and anti-Ter 119 antibody to detect granulocytes and erythroid lineage cells, respectively. The biotin conjugates were revealed with FITC-conjugated streptavidin. All antibodies were obtained from Pharmingen. Stained cells were analyzed with a FACscan (Becton-Dickinson) using CellQuest software.

Analysis of serum levels of immunoglobulin isotypes and immune responses

Studies of T-dependent and T-independent immune responses were performed as described previously (Sha et al. 1995). Six- to 7-week-old mice were injected with either alum-precipitated NP_{15}-CG (100 μg per mouse for T-dependent immune responses) or alum-precipitated NP-Ficoll (100 μg per mouse for T-independent immune responses). Sera were collected at day 7 for T-independent total immunoglobulin responses and at day 14 T-dependent immunoglobulin responses. Immunoglobulin specific for NP was analyzed with a sandwich enzyme-linked immunosorbent assay (ELISA) as described, with NP_{15}-BSA as the capturing antigen (Sha et al. 1995). To analyze immunoglobulin isotypes, sera were prepared from 6-week-old $ATM^{+/+}$ and $ATM^{-/-}$ littermates. Immunoglobulin isotypes were determined quantitatively against isotype standards using ELISA as described (Sha et al. 1995).

Southern blot analysis and PCR analysis of TCR rearrangement in lymphoma cells

Genomic DNA was purified from thymocytes and Southern blot analysis performed as described previously (Xu et al. 1996a). PCR analysis of TCR structure was performed as described (Winandy et al. 1995). PCR product was separated on a 1.2% agarose gel and assayed with Southern blot using an internal oligonucleotide probe. The PCR primers are: Dβ2.1, 5′-GTAGGCACCTGTGGGGAAGAAACT-3′; Jβ2.7, 5′-TGAGAGCTGTCTCCTACTATCGATT-3′; the oligonucleotide probe is 5′-ATTGTGGGGACTGGGGGGGC-3′.

Acknowledgments

We thank Drs. W. Sha, and J. Jacob for providing immunization reagents and helpful discussion, Dr. M.A. Handel for advice on histologic studies of spermatogenesis, A.W. Plug for help with meiotic studies, Drs. Peter Moens and Barbara Spyrogopholus for anti-Cor1 antibodies, and Brad Margus of the A-T Children's Project for his interest and support. This project was supported by National Institutes of Health (NIH) grants to D.B., CA-60592 to M.S.M. and GM-49779 to T.A. Y.X. was supported by a postdoctoral fellowship from the Cancer Research Fund of Damon Runyon-Walter Winchell Foundation. D.B. is an American Cancer Society research professor.

The publication costs of this article were defrayed in part by payment of page charges. This article must therefore be hereby

marked "advertisement" in accordance with 18 USC section 1734 solely to indicate this fact.

References

Ashley, T., A.W. Plug, J. Xu, A.J. Solari, G. Reddy, E.I. Golub, and D.C. Ward. 1995. Dynamic changes in Rad51 distribution on chromatin during meiosis in male and female vertebrates. *Chromosoma* **104:** 19–28.

Agamanolis, D.P. and J.I. Greenstein. 1979. Ataxia-telangiectasia: Report of a case with Lewy bodies and vascular abnormalities within cerebral tissue. *J. Neuropathol. Exp. Neurol.* **39:** 475–489.

Aguilar, M.J., S. Kamoshita, B.H. Landing, E. Boder, and R.P. Sedgwick. 1968. Pathological observations in ataxia-telangiectasia. A report on 5 cases. *J. Neuropathol. Exp. Neurol.* **27:** 659–676.

Anderson, C.W. 1993. DNA damage and the DNA-activated protein kinase. *Trends Biochem. Sci.* **19:** 433–437.

Baker, B.S. and A.T.C. Carpenter. 1972. Genetic analysis of sex chromosomal meiotic mutants in *Drosophila melanogaster*. *Genetics* **90:** 255–286.

Barlow, C., S. Hirotsune, R. Paylor, M. Liyanage, M. Eckhaus, F. Collins, Y. Shiloh, J.N. Crawley, T. Ried, D. Tagle, and A. Wynshaw-Boris. 1996. ATM-deficient mice: A paradigm of ataxia telangiectasia. *Cell* **86:** 159–171.

Bigbee, W.L., R.G. Langlois, M. Swift, and R.H. Jensen. 1989. Evidence for an elevated frequency of in vivo somatic cell mutations in ataxia telangiectasia. *Am. J. Hum. Genet.* **44:** 402–408.

Blackwell, K.T. and F.W. Alt. 1989. Molecular characterization of lymphoid V(D)J recombination activity. *J. Biol. Chem.* **264:** 0327–10330.

Blunt, T., N.J. Finnie, G.E. Taccioli, G.C. Smith, J. Demengeot, T.M. Gottlieb, R. Mizuta, A.J. Varghese, F.W. Alt, P.A. Jeggo, et al. 1995. Defective DNA-dependent protein kinase activity is linked to V(D)J recombination and DNA repair defects associated with the murine scid mutation. *Cell* **80:** 813–823.

Brown, E.J., P.A. Beal, C.T. Keith, J. Chen, T.B. Shin, and S.L. Schreiber. 1995. Control of p70 s6 kinase by kinase activity of FRAP in vivo. *Nature* **377:** 441–446.

Canman, C.E., A.C. Wolff, C.Y. Chen, A.J. Fornace Jr., and M.B. Kastan. 1994. The p53-dependent G1 cell cycle checkpoint pathways and ataxia-telangiectasia. *Cancer Res.* **54:** 5054–5058.

Cao, L., E. Alani, and N. Kleckner. 1990. A pathway for generation and processing of double-strand breaks during meiotic recombination in S. cerevisiae. *Cell* **61:** 1089–1101.

Cox, R., W.K. Masson, P.G. Debenham, and M.B.T. Webb. 1984. The use of recombinant DNA plasmids for the determination of DNA-repair and recombination in cultured mammalian cells. *Br. J. Cancer* (Suppl. VI) **46:** 67–72.

de Boer, P. and J.H. de Jong. 1989. Chromosome pairing and fertility in mice. In *Fertility and chromosome pairing: Recent studies in plants and animals* (ed. C.B. Gillies), pp. 37–76. CRC Press, Boca Raton, FL.

Dobson, M.J., R.E. Pearlman, A. Karaiskakis, B. Spyropoulos, and P.B. Moens. 1994. Synaptonemal complex proteins: Occurrence, epitope mapping and chromosome disjunction. *J. Cell. Sci.* **107:** 2749–2760.

Easton, D.F. 1994. Cancer risks in A-T heterozygotes. *Int. J. Radiat. Biol.* **66:** S177–S182.

Fehling, H.J., A. Krotkova, C. Saint-Ruf, and H. von Boehmer. 1995. Crucial role of the pre-T-cell receptor alpha gene in development of alpha beta but not gamma delta T cells. *Nature* **375:** 795–798.

Ganesh, A., P. North, and J. Thacker. 1993. Repair and misrepair of site-specific DNA double-strand breaks by human cell extracts. *Mutat. Res.* **299:** 251–259.

Gatti, R.A., I. Berkel., E. Boder, G. Braedt, P. Charmley, P. Concannon, F. Ersoy, T. Foroud, N.G. Jaspers, K. Lange, et al. 1988. Localization of an ataxia-telangiectasia gene to chromosome 11q22-23. *Nature* **336:** 577–580.

Greenwell, P.W., S.L. Kronmal, S.E. Porter, J. Gassenhuber, B. Obermaier, and T.D. Petes. 1995. TEL1, a gene involved in controlling telomere length in S. cerevisiae, is homologous to the human ataxia telangiectasia gene. *Cell* **82:** 823–829.

Hari, K.L., A. Santerre, J.J. Sekelsky, K.S. McKim, J.B. Boyd, and R.S. Hawley. 1995. The mei-41 gene of D. melanogaster is a structural and functional homolog of the human ataxia telangiectasia gene. *Cell* **82:** 815–821.

Hartwell, L.H. and M.B. Kastan. 1994. Cell cycle control and cancer. *Science* **266:** 1821–1828.

Jacobson, M. 1991. Histogenesis and morphogenesis of cortical structures. In *Developmental neurobiology*. 3rd ed. (ed. M. Jacobson), pp. 401–448. Plenum Press, New York, NY.

Janowski, M., R. Cox, and P.G. Strauss. 1990. The molecular biology of radiation-induced carcinogenesis: Thymic lymphoma, myeloid leukaemia and osteosarcoma. *Int. J. Radiat. Biol.* **57:** 677–691.

Jenkins, G. 1989. Chromosome pairing and fertility in plant hybrids. In *Fertility and chromosome pairing: Recent studies in plants and animals* (ed. C.B. Gillies), pp. 109–135. CRC Press, Boca Raton, FL.

Kastan, M.B., Q. Zhan, W.S. el-Deiry, F. Carrier, T. Jacks, W.V. Walsh, B.S. Plunkett, B. Vogelstein, and A.J. Fornace Jr. 1992. A mammalian cell cycle checkpoint pathway utilizing p53 and GADD45 is defective in ataxia telangiectasia. *Cell* **71:** 587–97.

Kato, R. and H. Ogawa. 1994. An essential gene, ESR1, is required for mitotic cell growth, DNA repair, and meiotic recombination in Saccharomyces cerevisiae. *Nucleic Acids Res.* **22:** 3104–3112.

Keegan, K.S., D.A. Holtzman, A.W. Plug, E.E. Brainerd, E.R. Christenson, N.J. Bentley, E.M. Taylor, M.S. Meyn, S.B. Moss, A.M. Carr, T. Ashley, and M. Hoekestra. The ATR and ATM protein kinases associate with different stages of meiotically pairing chromosomes. *Genes & Dev.* (this issue).

Khanna, K.K. and M.F. Lavin. 1993. Ionizing radiation and UV induction of p53 protein by different pathways in ataxia-telangiectasia cells. *Oncogene* **8:** 3307–3312.

Kirchgessner, C.U., C.K. Patil, J.W. Evans, C.A. Cuomo, L.M. Fried, T. Carter, M.A. Oettinger, and J.M. Brown. 1995. DNA-dependent kinase (p350) as a candidate gene for the murine SCID defect. *Science* **267:** 1178–1183.

Kitamura, D., A. Kudo, S. Schaal, W. Muller, F. Melchers, and K. Rajewsky. 1992. A critical role of lambda 5 protein in B cell development. *Cell* **69:** 823–831.

Kojis, T.L., R.A. Gatti, and R.S. Sparkes. 1991. The cytogenetics of ataxia telangiectasia. *Cancer Genet. Cytogenet.* **56:** 143–156.

Lin, W.C. and S. Desiderio. 1995. V(D)J recombination and the cell cycle. *Immunol. Today* **16:** 279–289.

McFarlin, D.E., W. Strober, and T.A. Waldmann. 1972. Ataxia-telangiectasia. *Medicine* **51:** 281–314.

Malissen, M., C. McCoy, D. Blanc, J. Trucy, C. Devaux, A.M. Schmitt-Verhulst, F. Fitch, L. Hood, and B. Malissen. 1986. Direct evidence for chromosomal inversion during T-cell receptor beta-gene rearrangement. *Nature* **319:** 28–33.

Meyn, M.S. 1993. High spontaneous intrachromosomal recombination rates in ataxia-telangiectasia. *Science* **260:** 1327–1330.

———. 1995. Ataxia-telangiectasia and cellular responses to DNA damage. *Cancer Res.* **55:** 5991–6001.

———. 1996. Chromosomal instability syndromes: Lessons for carcinogenesis. *Curr. Top. Microbiol. Immunol.* **221:** 71–148.

Mombaerts, P., A.R. Clarke, M.A. Rudnicki, J. Iacomini, S. Itohara, J.J. Lafaille, L. Wang, W. Ichikawa, R. Jaenisch, M.L. Hooper, and S. Tonegawa. 1992. Mutations in T-cell antigen receptor α and β block thymocyte development at different stages. *Nature* **360:** 225–231.

Morrow, D.M., D.A. Tagle, Y. Shiloh, F.S. Collins, and P. Hieter. 1995. TEL1, an S. cerevisiae homolog of the human gene mutated in ataxia telangiectasia, is functionally related to the yeast checkpoint gene MEC1. *Cell* **82:** 831–840.

Newcomb, E.W., M. Corominas, W. Bayona, and A. Pellicer. 1989. Multistage carcinogenesis in murine thymocytes: Involvement of oncogenes, chromosomal imbalances and T cell growth factor receptor. *Anticancer Res.* **9:** 1407–1415.

Pandita, T.K. and W.N. Hittelman. 1992. The contribution of DNA and chromosome repair deficiencies to the radiosensitivity of ataxia-telangiectasia. *Radiat. Res.* **131:** 214–223.

Paulovich, A.G. and L.H. Hartwell. 1995. A checkpoint regulates the rate of progression through S phase in S. cerevisiae in response to DNA damage. *Cell* **82:** 841–847.

Pecker, L., K.B. Avraham, D.J. Gilbert, K. Savitsky, G. Rotman, R. Hamik, T. Fukso, E. Schrock, S. Hirotsune, D. Tagle, F.S. Collins, A. Wynshaw-Boris, T. Ried, N.G. Copeland, N.A. Jenkins, Y. Shiloh, and Y. Ziv. 1996. Identification and chromosomal localization of *ATM*, the murine homolog of the ataxia-telangiectasia gene. *Genomics* (in press).

Peterson, R.D.A. and R.A. Good. 1968. Ataxia-telangiectasia. In *Birth defects–Immunologic deficiency disease in man.* (ed. D. Bergsma and R.A. Good), pp. 370–377. National Foundation, March of Dimes, New York, NY.

Plug, A.W., J. Xu, G. Reddy, E.I. Golub, and T. Ashley. 1996. Presynaptic association of Rad51 protein with selected sites in meiotic chromatin. *Proc. Natl. Acad. Sci.* **93:** 5920–5924.

Savitsky, K., A. Bar-Shira, S. Gilad, G. Rotman, Y. Ziv, L. Vanagaite, D.A. Tagle, S. Smith, T. Uziel, S. Sfez, et al. 1995. A single ataxia telangiectasia gene with a product similar to PI-3 kinase. *Science* **268:** 1749–1753.

Sedgwick, P.P. and E. Boder. 1991. Ataxia-telangiectasia. In *Hereditary neuropathies and spinocerebellar atrophies* (ed. J.M.B.V. deJong), pp. 347–423. Elsevier Science Publishing, New York, NY.

Sha, W.C., H-C. Liou, E.I. Tuomanen, and D. Baltimore. 1995. Targeted disruption of the p50 subunit of NF-κB leads to multifocal defects in immune responses. *Cell* **80:** 321–330.

Shiloh, Y. 1995. Ataxia-telangiectasia: Closer to unraveling the mystery. *Eur. J. Hum. Genet.* **3:** 116–138.

Shinkai, Y., S. Koyasu, K. Nakayama, K.M. Murphy, D.Y. Loh, E.L. Reiherz, and F.W. Alt. 1993. Restoration of T cell development in RAG-2-deficient mice by functional TCR transgenes. *Science* **259:** 822–825.

Spector, B.D., A.H. Filipovick, G.S. Perry III, and J.H. Kersey. 1982. Epidermiology of cancer in ataxia-telangiectasis. In *Ataxia-telangiectasia* (ed. B.A. Brodges, and D.G. Harden), pp. 103–138. Wiley and Sons, New York, NY.

Speed, R.M. 1982. Meiosis in the foetal ovary. I: An analysis at the light microscopy level using surface spreading. *Chromosoma* **85:** 427–437.

———. 1989. Heterologous pairing and fertility in humans. In *Fertility and chromosome pairing: Recent studies in plants and animals* (ed. C.B. Gillies), pp. 1–36. CRC Press, Boca Raton, FL.

Strober, W., R.D. Wochner, M.H. Barlow, D.E. McFarlin, and T.A. Waldmann. 1968. Immunoglobulin metabolism in ataxia telangiectasia. *J. Clin. Invest.* **47:** 1905–1915.

Sun, H.D, D. Treco, N.P. Schultes, and J.W. Szostak. 1989. Double-strand breaks at an initiation site for meiotic gene conversion. *Nature* **338:** 87–90.

von Boehmer, H. 1994. Positive selection of lymphocytes. *Cell* **76:** 219–228.

Weinert, T. and D. Lydall. 1993. Cell cycle checkpoints, genetic instability and cancer. *Semin. Cancer Biol.* **4:** 129–140.

Winandy, S., P. Wu, and K. Georgopoulos. 1995. A dominant mutation in the Ikaros gene leads to rapid development of leukemia and lymphoma. *Cell* **83:** 289–299.

Woods, C.G. and A.M. Taylor. 1992. Ataxia telangiectasia in the British Isles: The clinical and laboratory features of 70 affected individuals. *Q. J. Med.* **82:** 169–179.

Xu, Y. and D. Baltimore. 1996. Dual roles of ATM in cellular response to radiation and in cell growth control. *Genes & Dev.* (this issue).

Xu, Y., L. Davidson, F.W. Alt, and D. Baltimore. 1996a. Deletion of the Igκ light chain intronic enhancer/Matrix attachment region impairs but does not abolish VkJk rearrangement. *Immunity* **4:** 377–385.

———. 1996b. Function of the pre-T-cell receptor α chain in T-cell development and allelic exclusion at the T-cell receptor β locus. *Proc. Natl. Acad. Sci.* **93:** 2169–2173.

Zakian, V.A. 1995. *ATM*-related genes: What do they tell us about functions of the human gene? *Cell* **82:** 685–688.

Targeted disruption of ATM leads to growth retardation, chromosomal fragmentation during meiosis, immune defects, and thymic lymphoma.

Y Xu, T Ashley, E E Brainerd, et al.

Genes Dev. 1996, **10:**
Access the most recent version at doi:10.1101/gad.10.19.2411